Sensors and Materials, Vol. 38, No. 2 (2026) 761–774
MYU Tokyo

S & M 4346

Signal Enhancement Technology for Ultrasonic Guided Wave Monitoring of Rail Bottom Cracks Based on Spread Spectrum Technology

Wenhao Guo,[1*] Ziyi Zheng,[2] Nina Liu,[2,3] Yong Liu,[4] and Ping Wang[2]

[1]China Railway Fourth Survey and Design Institute Group Co., Ltd.,
745 Heping Avenue, Yangyuan, Wuchang, Wuhan 430063, China
[2]School of Automation, Nanjing University of Aeronautics and Astronautics,
29 Jiangjun Avenue, Jiangning District, Nanjing 211106, China
[3]Nanjing Vocational Institute of Railway Technology, 65 Pearl South Road, Pukou District, Nanjing 210031, China
[4]Nanjing PaiGuang High-Speed Transportation Intelligent Perception Research Institute Co., Ltd.,
8 Bailongjiang East Road, Jianye District, Nanjing 210017, China

(Received March 19, 2025; accepted September 1, 2025)

Keywords: rail crack detection, Barker code, ultrasonic guided wave, signal enhancement

In this paper, we address the challenge of detecting bottom cracks in railway tracks by proposing a signal enhancement technique designed to boost the signal-to-noise ratio of guided wave signals, thereby optimizing sensor performance. Utilizing Barker codes and binary phase shift keying technology, we modulated the original excitation signal to achieve spread spectrum processing and the subsequent despreading of received signals. This approach aims to overcome hardware and sensor limitations, enhancing the operational efficiency of the sensors used in ultrasonic guided wave detection systems. An experimental platform was established to test this technique on railway tracks with artificial bottom cracks of varying sizes. The results showed that the enhanced signals can travel further and detect cracks with a higher sensitivity than the original signals. This not only validates the effectiveness of our method in improving sensor capabilities but also supports the application of ultrasonic guided wave detection for bottom cracks in railway tracks.

1. Introduction

The safety of railway tracks is crucial to the railway transportation industry, as it not only concerns the safety of people's lives and property but also plays a key role in promoting economic growth, fostering technological innovation, and enhancing the national image.(1) Rail cracks usually originate from the surface or internal defects of the rail head and then gradually spread towards the rail waist, as shown in Fig. 1.(2,3) Once the crack develops to a certain extent, the track may break, which not only causes economic losses but may also lead to train derailment and significant casualties.(4,5)

*Corresponding author: e-mail: 19124295116@163.com
https://doi.org/10.18494/SAM5638

ISSN 0914-4935
https://myukk.org/

(a) (b) (c)

Fig. 1. (Color online) Actual cases of rail damage: (a) rail bottom rust, (b) lateral crack, and (c) broken rail.

Current rail inspection primarily relies on large-scale rail flaw detection vehicles, which, while effective, have certain limitations. Owing to the periodic nature of these inspections, the continuous monitoring of rail conditions cannot be achieved, potentially missing damage that occurs between inspection intervals.[6] Moreover, these vehicles cannot technically inspect the rail bottom for damage, making it difficult to effectively identify cracks and corrosion in this area.[7] Therefore, there is an urgent need to develop a new monitoring technology capable of the real-time monitoring of key areas prone to rail corrosion and crack initiation and the timely detection of potential damage to ensure the safety and reliability of railway transportation.

In response to these issues, scholars have employed ultrasonic guided wave detection technology for the real-time monitoring of rail breaks,[8] achieving promising experimental results. However, in practical applications, guided wave signals are inevitably subjected to various noise interferences, reducing the signal-to-noise ratio (SNR) and hindering the identification of rail bottom cracks. Thus, signal processing related to guided waves in rails is necessary.[9]

Spread spectrum technology, known for its strong anti-interference capabilities, was initially widely used in radar fields. Zhao and Cui[10] analyzed the anti-jamming mechanism of direct-sequence spread spectrum (DSSS) systems, laying the theoretical foundation for the analysis of DSSS's anti-jamming performance. Yao[11] defined two metrics for ultrasonic spread spectrum applications—energy efficiency and echo sequence correlation—and compared the parameter configurations of three modulation methods: binary phase shift keying (BPSK), binary frequency shift keying (BFSK), and binary amplitude shift keying (BASK). Widodo *et al.*[12] applied spread spectrum technology to the field of acoustic positioning to address outdoor mechanical positioning, reducing the impact of wind speed and machine noise on interference, proving that spread spectrum technology can ensure reliable signal transmission.

In recent years, the application of spread spectrum technology in the field of ultrasonic guided wave detection has continued to deepen. Yao *et al.*[13] investigated the optimization of Kasami sequences for coded excitation in guided ultrasonic wave testing for long rails, demonstrating their potential to enhance the SNR. Nenashev *et al.*[14] subsequently introduced modified nested Barker codes, highlighting their superior cross-correlation properties compared with Kasami sequences in applications involving ultra-wideband signals. Furthermore, Wang *et al.*[15] successfully integrated Kasami sequences with distributed optical fiber sensing (DOFS), enabling long-distance crack monitoring and validating their capability for dispersion resistance.

On the basis of the pulse compression method from communication principles, the excited signal is encoded with multiple chips instead of a single or short pulse signal. This method does not require an increase in the excitation voltage of the signal but improves the average excitation power by increasing the signal excitation time. Then, through related decoding methods, the energy of the excited signal is recompressed into a short pulse signal, ensuring that this method does not affect the resolution of signal crack identification and can significantly improve the system's SNR.[16]

In this study, we applied BPSK technology to the detection of rail bottom cracks using ultrasonic guided waves, leveraging the anti-interference capability of spread spectrum technology to enhance the SNR, thereby improving the detection sensitivity of ultrasonic guided waves to rail bottom cracks.

2. Methods

2.1 Signal spread spectrum and despreading

The main spread spectrum techniques include DSSS, frequency hopping spread spectrum (FHSS), and time hopping spread spectrum (THSS). DSSS technology expands the signal bandwidth by combining the original signal with a high-rate pseudo-random sequence code. This method increases the signal bandwidth by multiplying it with a pseudo-random sequence code. FHSS technology selects different frequency bands through a pseudo-random code, causing the carrier frequency to hop according to the changes in the pseudo-random sequence, thus expanding the signal spectrum. THSS is similar to frequency hopping but operates in the time domain, dividing the signal into multiple shorter time slots and deciding in which time slot to transmit the signal based on a pseudo-random sequence, thereby widening the signal spectrum.

Although FHSS can effectively expand the spectrum, it involves the frequency shift keying (FSK) of the carrier, making its hardware design relatively complex.[17] Therefore, in this paper, we have chosen DSSS.

The generation of DSSS signals relies on the modulation of direct sequence codes. Among the three modulation methods of FSK, amplitude shift keying (ASK), and phase shift keying (PSK), PSK has the lowest error rate.[18] Barker codes have good autocorrelation characteristics and require only a single excitation; hence, in this study, we selected Barker codes as the pseudo-random sequence code for spread spectrum technology.

An N-bit Barker code element $\left[x_0,\ x_1,\ \ldots,\ x_{(N-1)} \right]$ consists of "1" or "−1". When the code element is 1, the resulting waveform is in the same phase as the original waveform; when the code element is −1, the resulting waveform is opposite to the original waveform. The original waveform phase difference is π after two code elements, and several Barker codes form the pseudo-random binary spread spectrum code required for signal spread spectrum technology.

$$B\left[N\right]=\left[x_0,x_1,\ldots,x_{(N-1)}\right], x_i \in \left\{-1,1\right\} \tag{1}$$

For the decoding process after encoding, also known as pulse compression, the decoding process is actually the product of time width-bandwidth, that is, equivalent to the SNR gain after signal compression, and the SNR gain of the encoded signal is related to the code length N, so the SNR gain A_{SNR} after Barker code processing can be represented by the equation

$$A_{SNR} = 10 \times \log_{10} N, N \in \{2,3,4,5,7,11,13\}. \quad (2)$$

According to Eq. (2), to achieve the maximum SNR gain, the code element chooses a 13-bit Barker code.

Using DSSS technology, we multiply the information code *an* by the pseudo-random binary spread spectrum code $c(t)$ to obtain the composite code sequence $d(t)$. The carrier signal is modulated with the composite code sequence $d(t)$ to obtain the transmitted signal $S(t)$, using the pseudo-random code with a high rate to achieve the effect of spectrum expansion.[19] Ideally, the information code *an* is modulated to obtain the transmitted signal $S(t)$, and its equation is

$$S(t) = d(t)\sin(2\pi f_c t) = Aa_n c(t)\sin(2\pi f_c t), \quad (3)$$

where A represents the amplitude and f_c represents the center frequency of the carrier.

The pseudo-random spread spectrum code is a 13-bit Barker code. After the information and pseudo-random codes are multiplied, the composite code is obtained, and its frequency is expanded to 13 times the original frequency. The information code is "1", so the composite code is the same as the spread spectrum code. The spread spectrum sequence obtained after modulation is then used as the modulation encoding sequence and is modulated with a 200 kHz carrier signal $\sin(t)$ to obtain the carrier signal $S(t)$ after spread spectrum sequence modulation, which serves as the excitation signal. The ideal expanded spectrum process waveform is shown in Fig. 2. After the receiving end receives the signal, the received signal is calculated with the

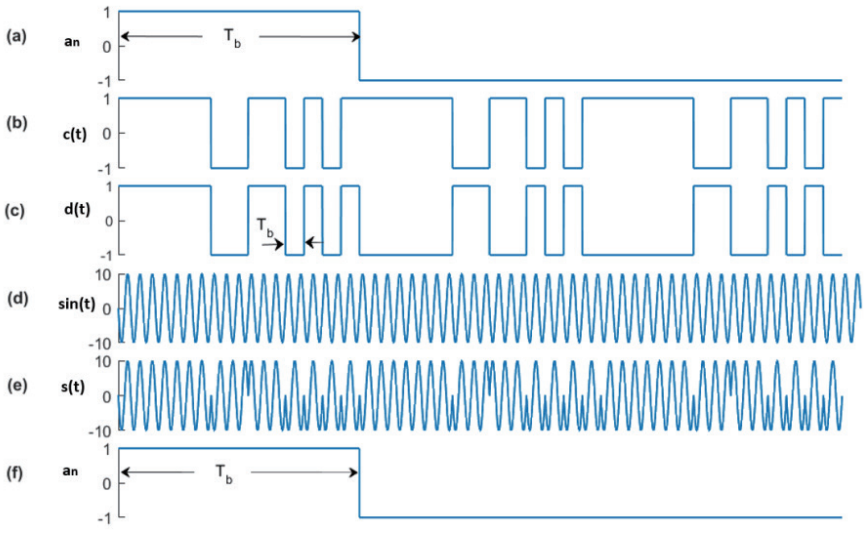

Fig. 2. (Color online) Waveform diagram of ideal spread spectrum process.

reference spread spectrum code, and after software filtering, the sent information code *an* can be restored.

The above spread spectrum and dispreading processes are all calculated and completed using MATLAB. The original signal is the Hanning window signal (HWS) wave. In MATLAB, DSSS technology is used to spread the HWS wave to obtain a new signal, called the direct-sequence signal (DSS) wave.

2.2 Verification of the feasibility of the spread spectrum method by simulation

By using the finite element simulation software ABAQUS/CAE, a three-dimensional model of the CHN60AT rail with a length of 1 m was established. The material properties of the model are as follows: mass density ρ = 7840 kg/m^3, Poisson's ratio σ = 0.29, and elastic modulus E = 210 GPa.

A crack detection model is established as shown in Fig. 3. The blue marks R_{pd}, E, and R_{pnd} simulate the piezoelectric sensors installed at the bottom of the rail. The middle position E is the excitation probe and the two sides are the receiving probes. The red box shows the cut artificial cracks at the bottom of the rail; the crack length is 150 mm, the depth is 10 mm, the width is 1.5 mm, and the crack distance from the end of the rail is L_1 = 423 mm, keeping L_2 = 5 mm unchanged. By changing the "R–E" spacing, that is, the distance between the excitation and receiving probes, the received signal propagation distance changes accordingly.

On the basis of the current detection requirements of the railway department for rail bottom crack depth, which is 10 mm, the size of the crack to be detected theoretically must be greater than half the wavelength of the detection frequency.[20] Therefore, a guided wave frequency of 200 kHz is selected.

As shown in Fig. 4, the starting interval of "R–E" spacing is 40 mm, and the step is increased by 20 mm until the "R–E" spacing is 140 mm. The HWS and DSS are used as the guided waves.

The simulation results of HWS are shown in Fig. 5, where V_{pnd} represents the nondamaged waveform and V_{pd} represents the waveform after cracking. Cracks cause significant amplitude attenuation to the propagation of a guided wave signal. With the increase in "R–E" spacing, the

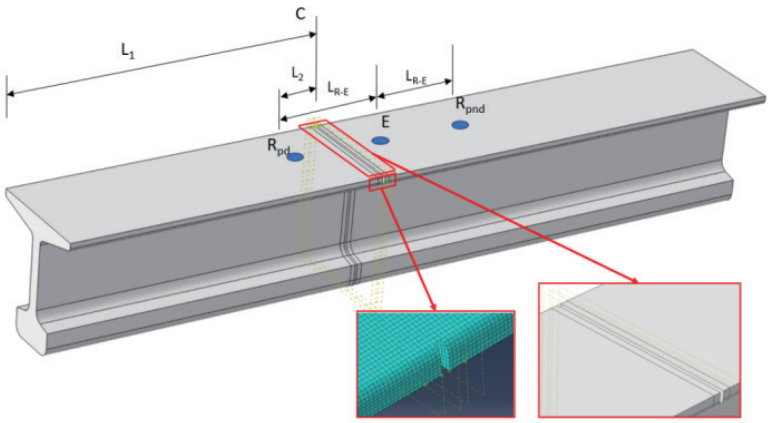

Fig. 3. (Color online) Ultrasonic guided wave rail bottom crack detection model.

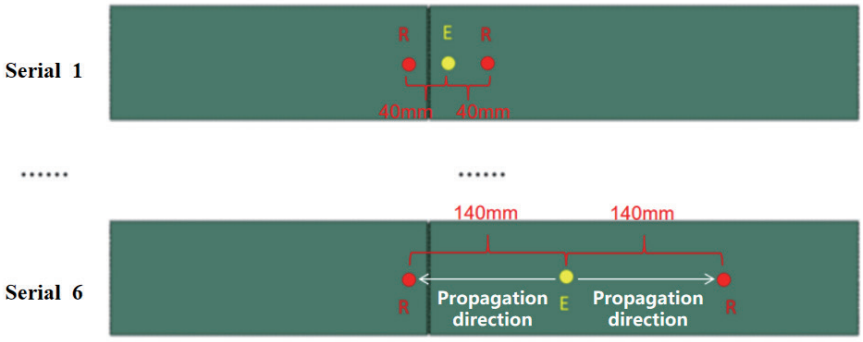

Fig. 4. (Color online) Emulation probe installation schematic.

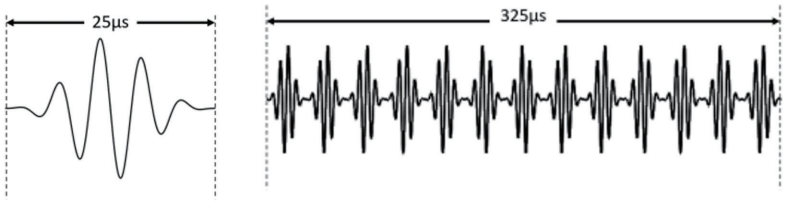

Fig. 5. Excitation signal.

propagation distance of the guided wave increases, and the amplitude of the received signal also attenuates.

The results obtained before and after the simulation of the DSSS excitation signal are shown in Figs. 6 and 7, respectively.

The signal that has not undergone deconvolution processing is denoted as S1. The unprocessed signal exhibits a distinct correlation peak, which corresponds to the information code "1" in the excitation signal. After the guided wave passes through a crack, the crack induces a certain degree of reflection and scattering, leading to the significant distortion and energy attenuation of the signal. Consequently, the correlation between the deconvolved signal and the original excitation signal weakens, making it impossible to fully recover the information code "1" from the excitation signal. The signal will not exhibit a high correlation peak, contrasting sharply with the processed signal of the direct wave that has not encountered any cracks.

As shown in Fig. 8, when the signal distance after deamplification increases to 100 mm, the propagation attenuation of V_{pnd} becomes clearer, but there is still a large difference between V_{pd} and V_{pnd}, which reduces the effect caused by the increase in propagation distance and further improves the detection range of cracks in the rail.

To describe the attenuation degree of the guided wave signal in the propagation process, the attenuation coefficient α_{pd} is used to represent it, and its equation is

$$\alpha_{pd} = 20\log_{10}\left(V_{pnd} / V_{pd}\right). \tag{4}$$

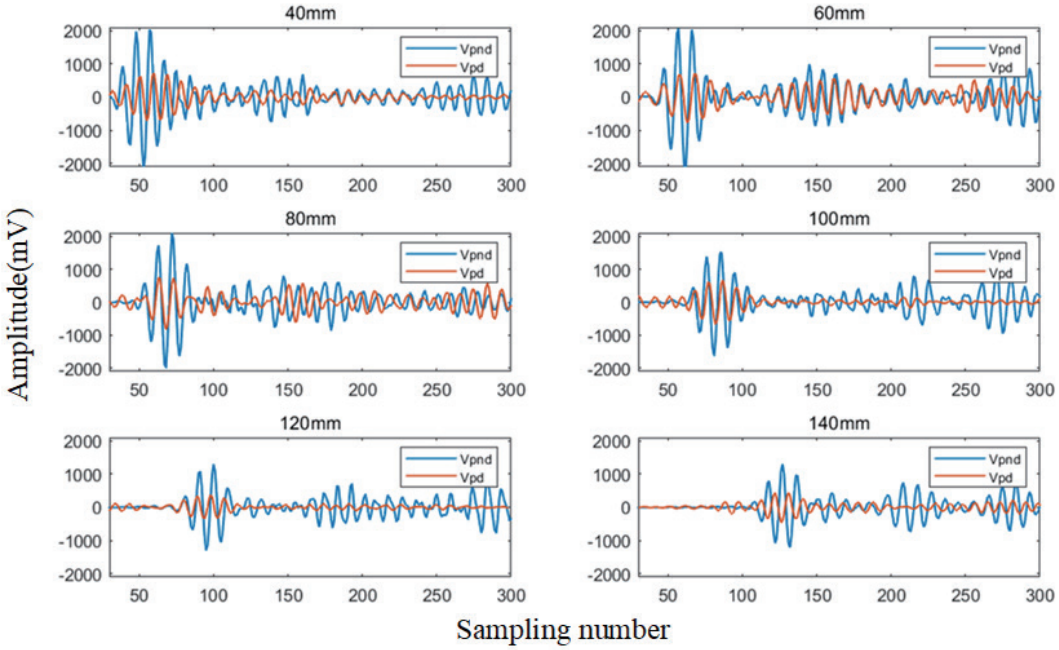

Fig. 6. (Color online) V_{pnd} and V_{pd} waveforms of HWS at different spacings.

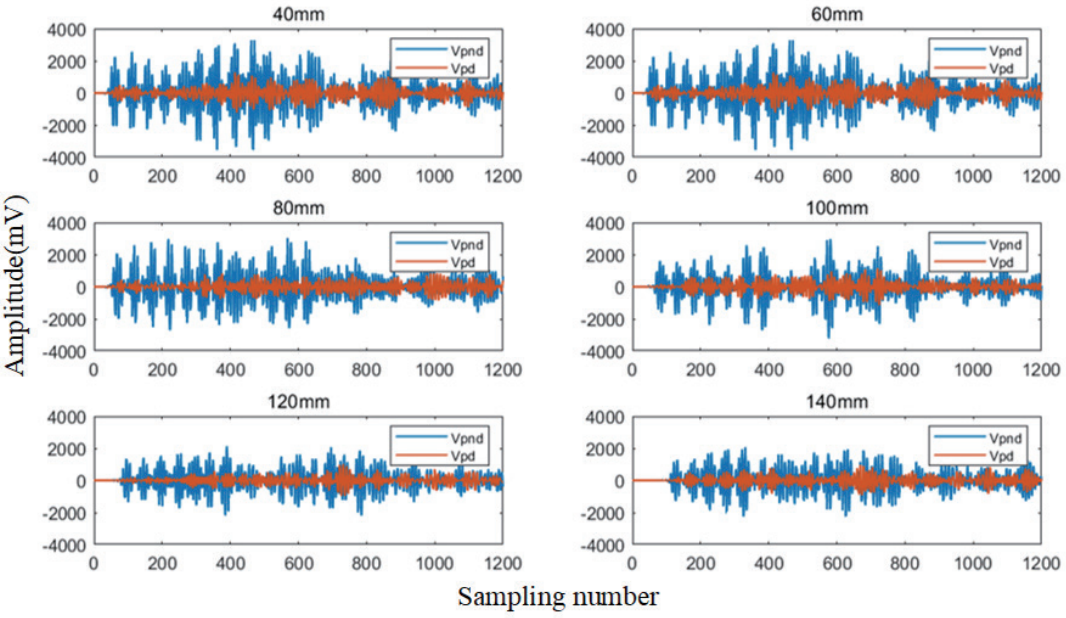

Fig. 7. (Color online) V_{pnd} and V_{pd} waveforms of unexpanded DSS.

The larger the attenuation coefficient α_{pd}, the more serious the amplitude attenuation of the signal after cracking. The attenuation coefficient α_{pd} of the signal S0 without spread spectrum processing is calculated from Table 1 to be 8.89 dB, whereas that of the signal S1 after spread spectrum processing is calculated from Table 2 to be 17.20 dB, and the average α_{pd} of the signal

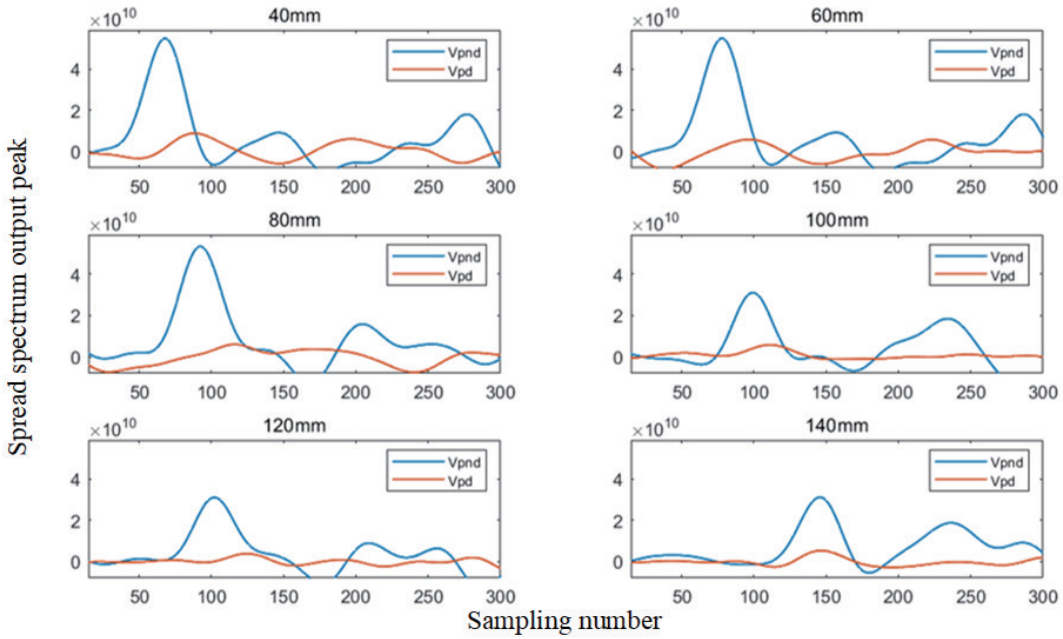

Fig. 8. (Color online) V_{pnd} and V_{pd} waveforms of DSS after deamplification.

Table 1
V_{pnd} and V_{pd} of HWS excitation waveform varying with distance.

No. (S0)	Interval (mm)	V_{pnd}	V_{pd}	α_L (dB)
1	40	2031.49	711.05	9.12
2	60	2030.34	719.08	9.02
3	80	2083.17	732.39	9.08
4	100	1509.10	656.73	7.23
5	120	1284.37	367.04	10.88
6	140	1107.31	440.77	8.00

Table 2
V_{pnd} and V_{pd} of DSS excitation waveform varying with distance.

No. (S1)	Interval (mm)	V_{pnd}	V_{pd}	α_{pd} (dB)
1	40	54.99	8.81	15.90
2	60	54.64	5.79	19.50
3	80	53.27	5.98	19.00
4	100	32.00	5.78	14.86
5	120	31.90	3.77	18.55
6	140	31.00	5.28	15.38

S1 after spread spectrum processing is increased by 8.31 dB. The results show that the cracks at the bottom of the rail are more easily detected after the HWS is processed by the spread spectrum technology.

In addition, the increase in propagation distance will also attenuate the guided wave signal. The attenuation degree of the propagation distance to the guided wave is expressed by the attenuation coefficient α_L, which is given as

$$\alpha_L = 20\log_{10}\frac{V_{pnd}\ (R - E_{min})}{V_{pnd}\ (R - E_{max})}. \tag{5}$$

Here, $V_{pnd}(R - E_{min})$ indicates the V_{pnd} amplitude at a distance of 40 mm and $V_{pnd}(R - E_{min})$ indicates the V_{pnd} amplitude at a distance of 140 mm.

The larger the attenuation coefficient α_L, the more serious the effect of distance attenuation on the guided wave signal. By analyzing the simulation results in Tables 1 and 2, the attenuation coefficient α_L of the signal without spread spectrum processing is calculated as 5.27 dB, whereas the attenuation coefficient α_L of the signal after spread spectrum processing is 4.73 dB, and the attenuation of the signal propagation after spread spectrum processing is reduced by 0.54 dB .

The simulation results showed that the spread spectrum technique can reduce the effect of distance attenuation on crack identification. At the same time, the amplitude of the signal decreases more after cracking, which increases the sensitivity of crack detection.

3. Experiment and Results

In this study, we employed piezoelectric ultrasonic transducers for guided wave excitation and reception in a custom-designed detection system. The experimental setup consists of three core modules: (1) a signal generation unit, (2) a data acquisition unit, and (3) the test specimen – a CHN60AT steel rail section of 1100 mm length.

To validate the system's detection capability, three artificial notch defects were precision-machined on the rail bottom surface. As illustrated in Fig. 9, these standardized flaws were positioned at 80 cm from the rail end, with each defect featuring the dimensional parameters shown in Fig. 9.

We employed ultrasonic transducers fabricated on the basis of the piezoelectric effect for the excitation and reception of ultrasonic guided waves. The overall ultrasonic guided wave detection system primarily consists of ultrasonic transducers, a signal generator, a power

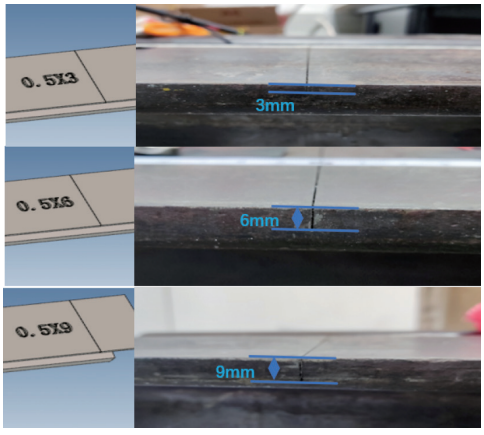

Fig. 9. (Color online) Artificial crack.

amplifier, an oscilloscope, and the steel rail under inspection. By utilizing a one-actuation dual-reception method, three 200 kHz ultrasonic guided wave transducers, R_{pd}, E, and R_{pnd}, were used, where E denotes the actuating probe, and R_{pd} and R_{pnd} represent the receiving probes. The steel rail was divided into two inspection sections: one with an artificial crack between R_{pd} and E, and the other without a crack between R_{pnd} and E, with the spacing between them being consistent with that of R_{pd} and E. For comparative experimentation, the spacing between R_{pd} and E is identical to that between R_{pnd} and E, and for ease of expression, both are referred to as "R–E" spacing. The relative positions of the probes with respect to the crack are illustrated in Fig. 10.

Using the conventional HWS and DSS as the excitation signals, we conducted three different "R–E" spacing experiments at the rail bottom crack detection platform for cracks of three different depths. The waveforms of the received DSSs after deconvolution processing are shown in Fig. 11.

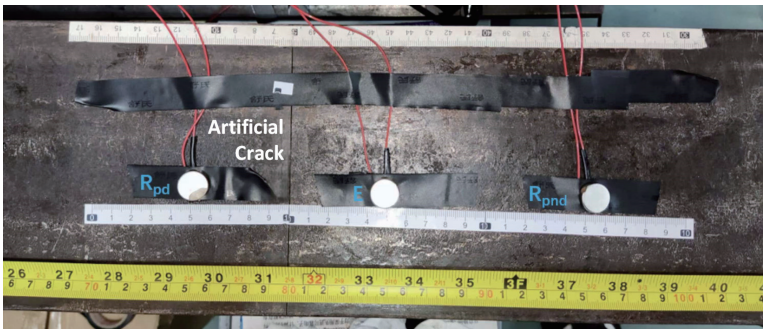

Fig. 10. (Color online) The probe is positioned relative to the crack.

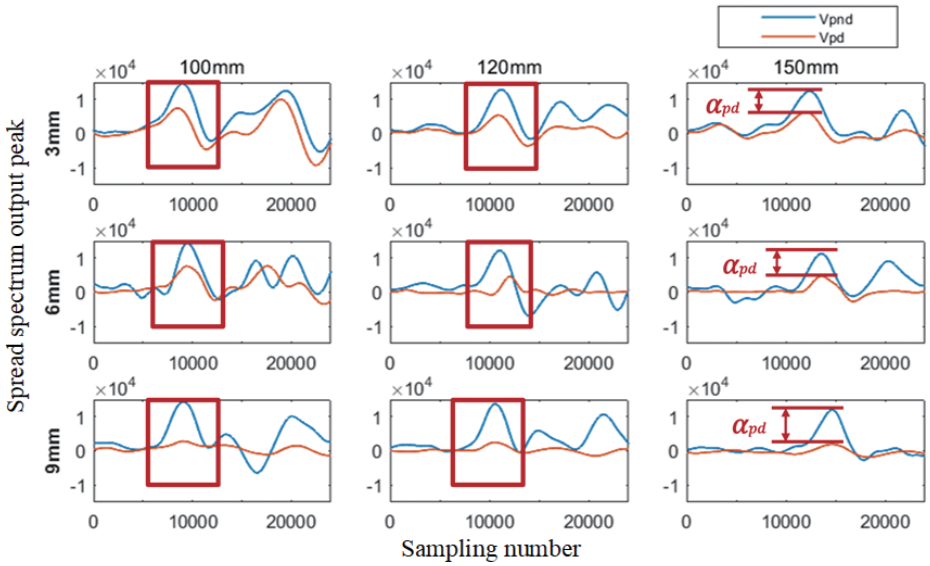

Fig. 11. (Color online) Deconvolved waveform of DSS received signal.

Figure 11 shows that under the bottom crack of the rail with depths of 3 and 6 mm, the median amplitude of V_{pd} and V_{pnd} is slightly attenuated in the time domain. According to the results of theoretical analysis, the detected crack size is guaranteed to be greater than half the frequency wavelength of the detected waveform, so the guided wave signal of the frequency used in the experiment is not sensitive to the bottom crack of the rail with a depth less than 7.5 mm. For the bottom crack of the rail with a depth of 9 mm, the amplitudes of V_{pd} and V_{pnd} decrease significantly compared with those of 3 and 6 mm, and the existence of the bottom crack of the rail can be detected stably.

Experiments with a crack depth of 9 mm were selected to show the amplitude changes of guided waves stimulated by HWS and DSS through the same crack size. Figure 12(a) shows the HWS without spread spectrum processing and Fig. 12(b) shows the waveform DSS calculated after spread spectrum processing.

As shown in Table 3, for the detection results of rail bottom cracks with a depth of 9 mm, the attenuation coefficient α_{pd} increases by 4.35, 1.601, and 5.6 dB at the "R–E" spacings of 100, 120, and 150 mm, respectively. Compared with the HWS excitation waveform, the attenuation coefficient α_{pd} of the spread-spectrum-processed signal increases by 3.847 dB, which proves that the method in this paper can make the guided wave signal more easily detect the cracks at the rail bottom.

As shown in Table 4, the attenuation coefficient α_L decreases to different degrees in three different experiments. Compared with the untreated signal attenuation coefficient α_L, the average decreases by 2.305 dB. The larger the attenuation coefficient α_L, the more serious the signal attenuation, indicating that this method can effectively reduce the effect of the guided wave caused by distance attenuation. Therefore, spread spectrum technology can effectively reduce the effect of distance attenuation on guided waves.

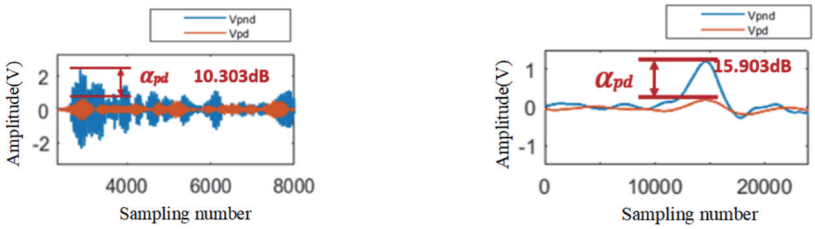

Fig. 12. (Color online) Comparison of attenuation coefficients obtained before and after spread spectrum processing: (a) HWS (before) and (b) DSS (after).

Table 3
Effect of spread spectrum processing on the attenuation coefficient α_{pd}.

Interval (mm)	Crack depth (mm)	HWS α_{pd} (dB)	DSS α_{pd} (dB)
100	9	9.715	14.065
120	9	13.156	14.757
150	9	10.303	15.903

Table 4
Effect of spread spectrum processing on the attenuation coefficient α_L.

Crack depth (mm)	HWS α_L (dB)	DSS α_L (dB)
3	4.437	1.424
6	3.943	2.121
9	3.642	1.562

4. Discussion and Conclusions

On the basis of the traditional ultrasonic guided wave detection, we used Barker codes as the pseudo-random sequence code and BPSK technology to encode and modulate the original HWS excitation signal to obtain a new excitation signal, and realized the spread spectrum processing of the excitation signal. Simulation and experiments on rail bottom artificial cracks (3, 6, and 9 mm) showed that this method reduces the guided wave signal distance attenuation by about 2.3 dB and increases the crack attenuation coefficient by about 3.8 dB. This improves the sensitivity for detecting small rail bottom cracks.

The 13-bit Barker code used in this study offers high real-time despreading in short-distance experiments, owing to its sharp autocorrelation peak and low hardware complexity. However, its limited sequence count (only 13 bits) makes it susceptible to intercode interference in multiprobe monitoring scenarios. Compared with Kasami sequences, which have a lower theoretical cross-correlation upper limit but a higher hardware complexity, and Gold codes, which provide more sequences but exhibit three-valued cross-correlation fluctuations, the Barker code presents a trade-off between performance and implementation complexity. Although recent studies combining CNN denoising with spread spectrum technology show promise in improving microcrack identification, they require substantial training data and computational resources. The BPSK despreading scheme in this study, with its simplicity and efficiency, better suits real-time railway monitoring. Guided wave dispersion remains a challenge for long-distance monitoring, and integrating dispersion compensation algorithms with BPSK modulation can enhance performance. For future long-distance applications, addressing distance attenuation and improving microcrack sensitivity will be crucial. Research into extending the Barker code's applicability through hybrid coding schemes or advanced signal processing techniques, while maintaining its low hardware complexity, can open new avenues for its use in railway monitoring.

Funding

This work was supported by the National Key Research and Development Program of China (grant number 2023YFB2603700), the authors sincerely acknowledge the support.

References

1 J. Liu, M. Geng, and B. Li: Urban Mass Transit **35** (2022) 129 (in Chinese).
2 J. Xing and J. Liang: J. Railway Tech. Innovation **1** (2025) 100 (in Chinese). https://doi.org/10.19550/j.issn.1672-061x.2024.10.12.004
3 L. Chen, H. Zhu, D. Wu, and Z. Zhang: New Mater. High-Speed Railway **2** (2023) 69 (in Chinese).
4 Y. Ma, X. Cui, P. Wang, Y. Gao, M. Han, and Y. Li: Appl. Acoust. **231** (2025) 110557. https://doi.org/10.1016/j.apacoust.2025.110557
5 P. W. Loveday, C. S. Long, and D. A. Ramatlo: Struct. Health Monit. **13** (2019) 1. https://doi.org/10.1177/1475921719893887
6 H. Pan, H. Wang, G. Tian, Z. Dong, F. Qiu, and B. F. Spencer: IEEE Sens. J. **19** (2019) 11050. https://doi.org/10.1109/jsen.2019.2934159.
7 Y. Yang, P. Wang, Y. Jia, L. Jing, S. Shi, H. Sheng, Y. Jiang, R. Liu, Y. Xu, and X. Li: Ultrasonics **136** (2024) 107164. https://doi.org/10.1016/j.ultras.2023.107164
8 D. Sun, W. Zhu, X. Qiu, L. Liu, Y. Xiang, and F. Z. Xuan: NDT & E Int. **135** (2023) 102788. https://doi.org/10.1016/j.ndteint.2023.102788
9 X. Zheng, Y. Yang, N. Hu, Z. Cheng, and J. Cheng: Mech. Syst. Signal Process. **214** (2024) 111400. https://doi.org/10.1016/j.ymssp.2024.111400
10 H. Zhao and J. Cui: Commun. Technol. **41** (2008) 38 (in Chinese).
11 Z. Yao: Pulse Coding Excitation and Transit Time Estimation for Ultrasonic Spread Spectrum Ranging (Tianjin Univ., Tianjin, 2010) p. 8 (in Chinese).
12 S. Widodo, T. Shiigi, N. M. Than, H. Kikuchi, K. Yanagida, Y. Nakatsuchi, Y. Ogawa, and N. Kondo: Eng. Agric. Environ. Food **7** (2014) 127. https://doi.org/10.1016/j.eaef.2014.04.001
13 W. Yao, Y. Yang, and X. Wei: Electronics **11** (2022) 1465. https://doi.org/10.3390/electronics11091465
14 V. A. Nenashev, A. R. Bestugin, A. V. Rabin, B. V. Solenyi, and S. A. Nenashev: Sensors **23** (2023) 9528. https://doi.org/10.3390/s23239528
15 Y. Wang, Y. Fan, J. Wang, W. Bai, R. Mei, X. Liu, and B. Jin: Opt. Fiber Technol. **94** (2025) 104316. https://doi.org/10.1016/j.yofte.2025.104316
16 H. Wang: Research on track failure detection Algorithm based on Barker coding excitation (Xi'an Univ. of Technol., Xi'an, 2020) p. 16 (in Chinese). https://doi.org/10.27398/d.cnki.gxalu.2020.000305
17 Q. Q. Lan, M. Dhanasekar, and Y. A. Handoko: Eng. Fail. Anal. **102** (2019) 170. https://doi.org/10.1016/j.engfailanal.2019.04.019
18 J. He, Y. Zhou, P. Qin, Y. Zhang, and S. Zhou: Rail Transp. Equip. Technol. **3** (2023) 127 (in Chinese). https://doi.org/10.13711/j.cnki.cn32-1836/u.2023.S2.031
19 H. Zhang: Research on the method of encoding excitation ultrasonic guided wave in long bone (Fudan Univ., Shanghai, 2014) p. 19 (in Chinese).
20 B. Jiang: Research on the method and experimental study of ultrasonic guided wave excitation in steel rails (Beijing Jiaotong Univ., Beijing, 2023) p. 20 (in Chinese). https://doi.org/10.26944/d.cnki.gbfju.2023.001235

About the Authors

Wenhao Guo received his B.S. degree from Lanzhou Jiaotong University, China, in 2008 and his M.S. degree from Southwest Jiaotong University, China, in 2011. From 2011 to 2025, he served as a senior engineer at the China Railway Fourth Survey and Design Institute Group Co., Ltd. His current research focuses on the monitoring, operation, and maintenance of key components in high-speed EMUs and urban rail transit vehicles. (19124295116@163.com)

Ziyi Zheng received her B.Eng. degree from Nanchang Hangkong University, China, in 2023 and has been studying in Nanjing University of Aeronautics and Astronautics, China, since 2023. Her current research interests are in turnout damage monitoring based on ultrasonic guided waves. (2433482737@qq.com)

Nina Liu received her B.Eng. degree in mechanical design, manufacturing, and automation from Lanzhou Jiaotong University, China, in 2005 and her M.Eng. degree in the same field from Nanjing Tech University, China, in 2011. She is currently a Ph.D. candidate in control science and engineering at Nanjing University of Aeronautics and Astronautics, China, with research focus on the intelligent operation and maintenance of mechanical systems. (911261415@qq.com)

Yong Liu received his B.S. degree from Southeast University, China, in 2008 and is pursuing his M.S. degree (research focus: modern sensing technology and precision instruments) at Nanjing University of Aeronautics and Astronautics. He currently serves as the Deputy Chief Engineer at Nanjing Paiguang High-Speed Transport Intelligent Perception Research Institute. His research interests cover automated detection technology, intelligent sensing for high-speed transport, and the standardization of NDT methodologies. (23804612@qq.com)

Ping Wang received his B.S., M.S., and Ph.D. degrees from Southeast University, China, in 1996, 1999, and 2004, respectively. His Ph.D. research focused on testing and measurement technology and virtual instruments. Since 2007, he has been a professor at Nanjing University of Aeronautics and Astronautics, China. His research interests include virtual instruments, wireless communication and radio frequency technology, and nondestructive testing and monitoring technology. (zeitping@nuaa.edu.cn)